Kaario, Ossi Tapani; Vuorinen, Ville; Kahila, Heikki; Im, Hong G.; Larmi, Martti

The effect of fuel on high velocity evaporating fuel sprays

Published in:
International Journal of Engine Research

DOI:
10.1177/1468087419854235

Published: 19/06/2019

Document Version
Publisher's PDF, also known as Version of record

Special Issue Article

International Journal of ENGINE RESEARCH

International J of Engine Research
2020, Vol. 21(1) 26–42

DOI: 10.1177/1468087419854235
journals.sagepub.com/home/jer
SAGE

The effect of fuel on high velocity evaporating fuel sprays: Large-Eddy simulation of Spray A with various fuels

Ossi Tapani Kaario[1], Ville Vuorinen[1], Heikki Kahila[1], Hong G Im[2] and Martti Larmi[1]

Abstract

Lagrangian particle tracking and Large-Eddy simulation were used to assess the effect of different fuels on spray characteristics. In such a two-way coupled modeling scenario, spray momentum accelerates the gaseous phase into an intense, multiphase jet near the nozzle. To assess fuel property effects on liquid spray formation, the non-reacting Engine Combustion Network Spray A baseline condition was chosen as the reference case. The validated Spray A case was modified by replacing *n*-dodecane with diesel, methanol, dimethyl ether, or propane assuming 150 MPa injection pressure. The model features and performance for various fuels in the under-resolved near-nozzle region are discussed. The main findings of the paper are as follows. (1) We show that, in addition to the well-known liquid penetration (L_{liq}), and vapor penetration (L_{vap}), for all the investigated fuels, the modeled multiphase jets exhibit also a third length scale L_{core}, with discussed correspondence to a potential core part common to single phase jets. (2) As a characteristic feature of the present model, L_{core} is noted to correlate linearly with L_{liq} and L_{vap} for all the fuels. (3) A separate sensitivity test on density variation indicated that the liquid density had a relatively minor role on L_{liq}. (4) Significant dependency between fuel oxygen content and the equivalence ratio (Φ) distribution was observed. (5) Repeated simulations indicated injection-to-injection variations below 2% for L_{liq} and 4% for L_{vap}. In the absence of experimental and fully resolved numerical near-nozzle velocity data, the exact details of L_{core} remain as an open question. In contrast, fuel property effects on spray development have been consistently explained herein.

Keywords

Large-Eddy simulation, Lagrangian particle tracking, Engine Combustion Network, Spray A, fuel comparison, liquid length

Date received: 12 October 2018; accepted: 9 May 2019

Introduction

Engine Combustion Network (ECN) is an international collaborative effort to focus research and to facilitate experimental and computational data access within the engine combustion context.[1,2] A focal topic within ECN is spray combustion which is approached by detailed measurements and simulations on *n*-dodecane, *n*-heptane, and gasoline. One of the best documented diesel combustion target conditions is the ECN Spray A case in which liquid *n*-dodecane is injected through a nozzle hole (D = 90 μm) at a high injection pressure (150 MPa) in engine relevant conditions (T = 900 K, P = 6 MPa). Experimental, non-reacting ECN spray cases have been used as reference cases for many numerical studies[2–12] utilizing Lagrangian particle tracking (LPT), Large-Eddy simulation (LES), or Reynolds-averaged Navier–Stokes (RANS) turbulence modeling (see Table 1). Here, we use the non-reacting Spray A target condition as the baseline validation case. In addition, in the present numerical investigations, we extend the Spray A case by replacing *n*-dodecane with various other fuels to better understand fuel property effects on spray characteristics.

[1]Department of Mechanical Engineering, School of Engineering, Aalto University, Espoo, Finland
[2]Clean Combustion Research Center, King Abdullah University of Science and Technology, Thuwal, Saudi Arabia

Corresponding author:
Ossi Tapani Kaario, Department of Mechanical Engineering, School of Engineering, Aalto University, 00076 Aalto, Finland.
Email: ossi.kaario@aalto.fi

Table 1. Examples of ECN-related modeling studies using two-way or four-way coupling within the Lagrangian spray modeling context.

Investigators	Year	Formulation	SGS model	Droplet breakup	Turbulent dispersion	Four-way coupling	Reacting
Bhattacharjee and Haworth[3]	2013	URANS	–	Yes	Yes	No	Yes
Pei et al.[4]	2015	URANS	–	No	Yes	No	Yes
Xue et al.[5,a]	2015	URANS	–	Yes	Yes	Yes	No
Blomberg et al.[6]	2016	URANS/LES	–/$k-l$	Yes	Yes	No	Yes
Xue et al.[7]	2013	URANS/LES	–/Various	Yes	Yes	Yes	No
Irannejad and Jaberi[8]	2015	LES	$k-l$	Yes	Yes	No	No
Gong et al.[9]	2014	LES	$k-l$	Yes	Yes	No	Yes
Pei et al.[10]	2015	LES	Dyn. struct.	Yes	Yes	Yes	Yes
Wehrfritz et al.[11]	2016	LES	ILES	Yes	No	No	Yes
Kahila et al.[12]	2018	LES	ILES	Yes	No	No	Yes

SGS: subgrid scale; LES: Large-Eddy simulation; VOF: volume of fluid; LPT: Lagrangian particle tracking; URANS: Unsteady RANS; ILES: Implicit LES.
[a]VOF and LPT were compared.

In modern diesel engines, fuel is injected directly into the cylinder using a common-rail injection system. After the start of injection, the liquid phase reaches a maximum penetration length, commonly termed the liquid length (L_{liq}) that remains nearly constant during the steady period of injection. The tip of the vapor phase (L_{vap}) penetrates downstream with the well-established scaling $L_{vap} \sim \sqrt{t}$, where t indicates time. It has been reported that L_{liq} depends on the ambient and fuel injection conditions.[13] For example, Siebers [14] showed that L_{liq} is ultimately limited by mixing, that is, the mixing rate of ambient energy and mass into the spray will determine the rate of liquid fuel evaporation. Optimally, fuel is fully evaporated before reaching the cylinder walls. However, at low ambient temperature, the liquid phase can reach the cylinder walls leading to wall wetting.[15–18] Thereby, in the context of engine development process, it is essential to predict fuel property effects on L_{liq}.

With relevance to the present study, some key fuel properties are (1) liquid fuel density ρ_f, (2) latent heat h_f, and (3) vapor pressure P_f. Latent heat h_f has a significant effect on the gas phase (and liquid phase) temperature during the evaporation process. Vapor pressure (or boiling point), on the contrary, has an important role in the fuel evaporation rate.[19] In practice, the higher the P_f, the faster the liquid evaporates. If P_f of a fuel reaches the ambient pressure, it starts to boil. Experimentally, a positive correlation has been observed between L_{liq} and the fuel boiling point temperature.[20] Thereby, a low boiling point fuel evaporates quickly and the liquid length is shorter than that of a high boiling point fuel.[21,22] It is noted that in engine relevant conditions (high ambient pressure), boiling does not typically take place. A scaling law for liquid penetration[14] shows that fuel density correlates with liquid length $L_{liq} \sim \sqrt{\rho_f/\rho_a}$, where ρ_a is the ambient gas density. In the validation of the scaling law, the density ratio ranged between $13 < \rho_f/\rho_a < 220$.[14] Here, the span of the investigated density ratios is $20 < \rho_f/\rho_a < 34$.

There are several computational studies on single fuel LES/LPT (see Table 1). However, we are aware of only a few papers addressing the fuel property effects on spray characteristics. For example, several studies are available concerning detailed single fuel inner-nozzle simulations.[23–25] Som et al.[26] used RANS modeling for both the inner-nozzle and the ambient part of the injector comparing biodiesel and standard diesel fuels. They concluded that biodiesel has both higher liquid length and vapor penetration than standard diesel. The observation was explained by the high boiling point temperature and heat of vaporization of biodiesel. While the discussed studies were carried out in non-reacting conditions, there are a number of detailed numerical investigations carried out in reacting conditions as well.[4,8,9] One of the few studies which included fuel property comparison in reacting conditions was carried out by Som and Longman.[27] The study was an extension to the earlier non-reacting study.[26] They compared biodiesel to petrodiesel and pointed out the need to develop better surrogates for the considered fuels.

According to the previous literature[7,9,28,29] the schematic picture in Figure 1 summarizes typical LES/LPT spray centerline average velocity and temperature profiles at distances $z/D < 200$ from the nozzle exit. We emphasize that this graph is solely based on simulations while respective experimental data are presently not available. Next, we discuss some of the features in the figure. The domain in Figure 1 consists of three parts. (1) Droplets lose their momentum accelerating the gaseous phase, denoted as L_I in Figure 1. At the border between L_I and L_{II}, the maximum axial gas phase velocity is reached, and the droplets have lost most of their momentum. Since droplet–gas phase interaction is governed by the Stokes number[19] ($St = \tau_p U/D$, where $\tau_p = \rho_f d^2/18\mu_g$, U is the characteristic velocity, d is the droplet diameter, and μ_g is the molecular gas viscosity), it is expected that within L_I, St number dictates the acceleration of gas phase and the respective deceleration of droplets. Increasing St number implies reduced rate of momentum transfer from droplets to gas phase and, hence, increased L_I. In addition, droplet evaporation is initialized which has a cooling effect on the gas phase. (2) At the beginning of L_{II}, the slip velocity is low. While the core of the jet is still unaffected by the shear layer, the potential core or spray core (L_{core}) is established at the centerline of the spray analogous with the findings on single phase jets.[30] The length of L_{II} is related to the diameter of the gas jet at the end of L_I. (3) After the grown instabilities have reached the spray axis at the end of L_{II}, the mixing governed velocity decay starts. Based on momentum and mass conservation, the axial velocity decays in single phase jets as $U \sim 1/z$. In addition, due to mixing, the spray centerline temperature starts to increase towards the ambient gas phase temperature. In the absence of experimental and fully resolved numerical near-nozzle velocity data, Figure 1 only indicates typical LES/LPT modeling outcome. For future development of such models, we propose that the connection between L_{core}, L_I, and L_{II} needs to be better understood for various fuels.

Thereby, the following hypothesis are formulated for the present numerical work: (1) liquid length between the studied fuels is proportional to L_{core}, that is, $L_{liq} \sim L_{core}$, since the mixing of hot gases into the spray core starts only after L_{core}; (2) liquid length is also affected by other properties, such as liquid density, heat of vaporization, or vapor pressure, that is, $L_{liq}(\rho_f, h_f, P_f, \ldots)$; and (3) vapor penetration is proportional to L_{core}, that is, $L_{vap} \sim L_{core}$, after the beginning of the mixing zone (beginning of L_{III}), the vapor jet penetrations are similar.

As discussed above and summarized in Table 1, there are not many detailed numerical studies assessing fuel property effects on spray characteristics. With relevance to engine R&D process, understanding LES/LPT model performance for various fuels is important. Therefore, our aim is to bridge the observed research gap by computational LES/LPT modeling of

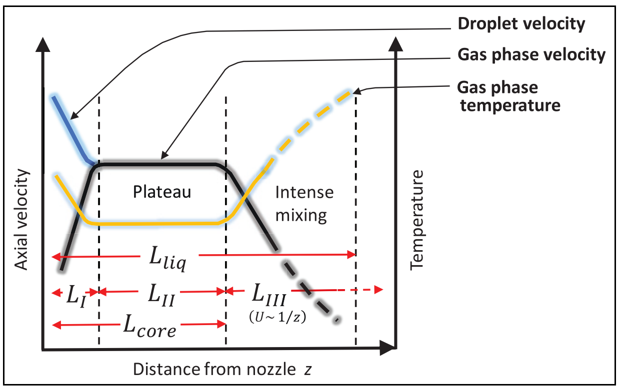

Figure 1. Schematic representation of the gas phase temperature, droplet velocity, and gas phase velocity development at the spray centerline for the near-nozzle region. $L_{core} = L_I + L_{II}$. The schematic is constructed based on computational studies on LES/LPT.[7,9,28,29]

the mixing and evaporation characteristics of various fuels. In order to answer the above stated research hypotheses, the below objectives have been formulated for the present numerical study:

1. Validate the LES model in the non-reacting ECN Spray A case for *n*-dodecane;
2. Compare diesel, dimethyl ether (DME), methanol, and propane to *n*-dodecane in the Spray A conditions;
3. Asses injection-to-injection variation between the fuels;
4. Understand the effect of liquid density on liquid length;
5. Analyze the local equivalence ratio differences between the fuels.

In larger context, the model features and performance for various fuels in the under-resolved near-nozzle region are discussed. In order to answer the objectives, the study is limited to non-reacting sprays. However, we note that the near-field metrics of non-reacting and reacting Spray A are essentially the same.[12]

Governing equations

Fluid motion

The governing equations for the gaseous phase describe the conservation of mass, momentum, energy, and species mass fractions, and they are written as follows

$$\frac{\partial \rho}{\partial t} + \frac{\partial \rho u_j}{\partial x_j} = 0 \tag{1}$$

$$\frac{\partial \rho u_i}{\partial t} + \frac{\partial \rho u_i u_j}{\partial x_j} = -\frac{\partial}{\partial x_j}\left(p\delta_{ij} - \tau_{ij}\right) + M_d \tag{2}$$

$$\frac{\partial \rho h}{\partial t} + \frac{\partial \rho u_j h}{\partial x_j} = -\frac{\partial}{\partial x_j}\left(\tau_{ij} u_j\right) + \frac{\partial}{\partial x_j}\left(\lambda \frac{\partial T}{\partial x_j}\right) + M_h \tag{3}$$

$$\frac{\partial \rho Y_k}{\partial t} + \frac{\partial \rho u_j Y_k}{\partial x_j} = \frac{\partial}{\partial x_j}\left(\rho D_k \frac{\partial Y_k}{\partial x_j}\right) + M_Y \tag{4}$$

where M_d is the momentum source term exerted from the droplets to the gas phase, M_h is the energy source from droplets, and M_Y denotes the vapor mass source term from the liquid phase (here Y refers to the fuel, depending on the case).

In LES, equations (1)–(4) are spatially filtered resulting in additional subgrid-scale (sgs) terms from the non-linear part of the equations and they can be written in the form $NS(\tilde{\rho}, \tilde{u}_i, \ldots) = \tau_{sgs}$. The sgs terms, which require further modeling efforts, account for the interaction between the resolved and the unresolved scales. In addition, according to the Boussinesq hypothesis, viscosity can be written as $\mu = \mu_g + \mu_t$, where μ is the total viscosity, μ_g is the molecular viscosity obtained from Sutherland's law,[31] and μ_t is the turbulent viscosity calculated from

Table 2. Operating conditions for Spray A.

Ambient conditions	
O_2	0%
Pressure	6 MPa
Temperature	900 K
Density	22.8 kg/m^3
Injector conditions	
Fuel injection temperature[a]	363/323 K
Nozzle diameter	90 μm
Injection pressure	150 MPa

DME: dimethyl ether.
[a]Diesel and *n*-dodecane values are given at $T = 363$ K, and DME and propane are at $T = 323$ K.

$$\mu_t = c_1 \rho \Delta k_{sgs}^{1/2} \tag{5}$$

In equation (5), Δ denotes the filter width calculated from the cell volume V_{cell} as $\Delta = V_{cell}^{1/3}$. The present study uses a $k - l$ model[32] for the sgs where a transport equation for the sgs turbulent kinetic energy k_{sgs} is solved according to

$$\frac{\partial \rho k_{sgs}}{\partial t} + \frac{\partial \rho u_j k_{sgs}}{\partial x_j} = P - \rho \varepsilon_{sgs} + \frac{\partial}{\partial x_j}\left(\mu_t \frac{\partial k_{sgs}}{\partial x_j}\right) \tag{6}$$

where P is the production term calculated as follows

$$P = \tau_{sgs,ij} \frac{1}{2}\left(\frac{\partial u_i}{\partial x_j} + \frac{\partial u_j}{\partial x_i}\right) \tag{7}$$

and ε_{sgs} is the sgs dissipation rate of the turbulent kinetic energy

$$\varepsilon_{sgs} = c_2 \frac{k_{sgs}^{3/2}}{\Delta} \tag{8}$$

The coefficients c_1 and c_2 have the values 0.05 and 1.0, respectively.[29,33] A second-order accurate flux limited scheme is used for the spatial discretization, while a second-order accurate three-time level method is applied for the time integration.[34] The mathematical closure for the system of equations is provided by the ideal gas law. Simulations have been carried out with the Star-CD 4.24 code.

Droplet motion

In LPT, the motion of individual droplets is tracked through the computational domain. The number of droplets in a diesel spray can be significant and, hence, it is a common practice to reduce the computational cost and group droplets with similar properties into a "parcel." In this study, parcels have equal mass indicating that the number of the droplets within a parcel is varying depending on the droplet size. The parcel position is updated from

$$\frac{dx_p}{dt} = u_p \tag{9}$$

It is assumed that the force acting on a droplet is due to the aerodynamic drag, leading to the following formulation under assumption of spherical droplets[19]

$$\frac{du_p}{dt} = \frac{C_d}{\tau_p}\frac{Re_p}{24}\left(u_g - u_p\right) \tag{10}$$

The expression for the drag coefficient C_d is given as follows

$$C_d = \begin{cases} \frac{24}{Re_p}\left(1 + \frac{1}{6} Re_p^{2/3}\right) & Re_p < 1000 \\ 0.424 & Re_p \geqslant 1000 \end{cases} \tag{11}$$

where Re_p is the droplet Reynolds number based on the droplet slip velocity.

The parcels are advanced in time using a semi-implicit time integration method by taking five subiterations within each time step. The momentum source term M_d in equation (2) is evaluated for each cell separately by considering all the parcels within the cell. The following relation for the source term is assumed[19]

$$M_d = \frac{1}{2}\rho_g C_d A \left|u_g - u_p\right|\left(u_g - u_p\right) \tag{12}$$

where A is the projected droplet area.

Concerning droplet breakup modeling, Wehrfritz et al.[28] observed in Spray A conditions (see Table 2) that droplet breakup takes place only upto $\sim 20D$ (nozzle hole diameter D) from the nozzle exit after which the droplet Weber number becomes too small for droplet breakup to take place. In addition, it has been numerically observed that droplet Sauter mean diameter (SMD) reduces very quickly (within ~1–2 mm) below 1 μm level.[28,35] Experimental evidence in non-evaporating Spray A conditions also indicates very quick droplet SMD reduction to 1 μm level.[36] On the contrary, detailed experimental information on evaporating droplet sizes in Spray A conditions using *n*-dodecane is still missing, let alone droplet sizes for other fuels (such as those studied here).[1,2] Considering the above limitations, we apply a constant droplet size (Weber number $We < 12$) at the nozzle exit without a droplet breakup model for all tested fuels with the aim to reduce ambiguity related to droplet breakup modeling with various fuels. Similar approach has been utilized in a spray LES simulation by Kaario et al.[37] Thus, we aim to decrease the uncertainties related to the comparison between the various fuels. Neither droplet collision nor turbulent dispersion modeling is applied in the present work in similar fashion as in previous works.[11,28,33,37]

Droplet evaporation

The mass transfer from the droplets due to evaporation is modeled according to Bird et al.[38] The rate of change of the droplet mass is given as follows

$$\frac{dm_d}{dt} = -A_dK_gp_g\ln\left(\frac{p_g - p_{v,\infty}}{p_g - p_{v,d}}\right) \quad (13)$$

where A_d is the droplet surface area, K_g is the mass transfer number, p_g is the gas pressure, $p_{v,\infty}$ is the vapor pressure in the droplet surroundings, and $p_{v,d}$ is the vapor pressure at the droplet surface. The mass transfer coefficient K_g is modeled according to Ranz and Marshall[39] and it is given as follows

$$K_g = \frac{ShD_m}{R_mT_md} \quad (14)$$

where Sh is the Sherwood number, D_m the vapor–gas mixture diffusivity, R_m the mixture gas constant, and T_m is the mixture temperature. The heat transfer at the droplet surface is derived from the droplet energy balance and the Ranz–Marshall correlations for Sh and Nusselt (Nu) number[39] are applied in the equations for mass and heat transfer. The droplet evaporation time can be expressed as $dm_d/dt = -m_d/\tau_e$ where the evaporation time is as follows

$$\tau_e = \frac{\rho_d d^2}{6D_mSh\rho_g\ln\left[\left(p_g - p_{v,\infty}\right)/\left(p_g - p_{v,d}\right)\right]} \quad (15)$$

Computational setup

The present study uses the ECN Spray A case as the baseline case. The Spray A experiments have been conducted with n-dodecane ($n{-}C_{12}H_{26}$). A fuel comparison is carried out for four additional fuels: diesel, methanol, DME, and propane. The non-reacting case selected here uses a mixture consisting of 0% O_2 content in 900 K ambient temperature together with 150 MPa injection pressure and 90 μm nozzle hole diameter. Details of the operating conditions in the present fuel comparison are given in Table 2.

The most relevant fuel properties are provided in Table 3. The properties of liquid diesel have been taken from the literature[40,41] and those of DME from Teng et al.[42] The properties of n-dodecane, methanol, and propane are taken from the NIST database.[43] The stoichiometric mixture fraction values have been calculated by assuming an oxidizer mixture with 21% of O_2. It is seen that there is a large variation in the liquid density between the fuels ranging between 784 and 449.8 kg/m^3 at the injection temperature. Figure 2(a) shows the temperature sensitivity of the liquid density for all the five fuels. Vapor pressure affects significantly the evaporation process as seen from equation (13). Figure 2(b) shows the vapor pressures of the fuels as a function of temperature. Large differences are observed also in this quantity. According to hypothesis 2, the liquid length will also be affected by vapor pressure. Due to the very low boiling point temperature of DME and propane, their injection temperature was set to $T = 323$ K. This is in line with liquid propane experiments comparing light fuel oil (LFO) and propane sprays in a room temperature spray bomb.[44] In those experiments, it was necessary to decrease the injection temperature of propane due to fast vaporization inside the nozzle.

The injection velocity versus time profile of n-dodecane is obtained from experimental massflow profile (from CMT-Motores Térmicos (CMT) virtual profile generator)[1]. Figure 3 shows the injection velocity profiles for the studied five fuels. In the present study, the same injection pressure is used for all fuels (see Table 2). Therefore, the injection velocity for each fuel depends on its density according to $U_i \sim \sqrt{2\Delta p/\rho_i}$, where Δp is the pressure difference over the nozzle orifice and ρ_i is the liquid density (i refers to diesel, methanol, n-dodecane, DME, or propane). Since fuel mass flow rate is calculated from $\dot{m}_i = \rho_iA_DU_i$, where A_D is the nozzle hole area, $\dot{m}_i$ also varies between the fuels. The total injected fuel mass at $t = 1.5$ ms for each fuel is shown in Table 4.

Recent DNS of Spray A[35] combining inner-nozzle simulation and the subsequent spray modeling using the volume of fluid (VOF) method suggests that at 1 mm distance from the nozzle exit the droplet sizes are very small, SMD = 0.5 μm being most probable. As explained previously in section "Droplet motion," the present study utilizes a constant droplet size (i.e. $We < 12$) at the nozzle exit without a droplet breakup model. In accordance with DNS of Spray A[35] and LES of Spray A,[28] we use 0.5 μm constant droplet size at the nozzle exit for all the simulated fuels. For reference, the total number of parcels in the present study is 1.2×10^6 (at $t = 1.5$ ms).

Table 3. Fuel properties.

Fuels	Diesel	Methanol	n-dodecane	DME	Propane
Chemical formula	$C_{16}H_{34}$	CH_3OH	$C_{12}H_{26}$	C_2H_6O	C_3H_8
Molecular weight (g/mol)	226	32	170	46	44
Density[a] (kg/m^3)	784	722.1	697.5	612	449.8
Vapor pressure[a] (Pa)	2137	2.56×10^5	1233	1.19×10^6	1.71×10^6
Latent heat[a] (kJ/kg)	260.3	1046.9	325.9	356.9	285.3
Viscosity[a] (kg/ms)	8.8×10^{-4}	2.4×10^{-4}	5.6×10^{-4}	1.3×10^{-4}	7.4×10^{-5}
Critical temperature (K)	658	513	658	400	369.8
Critical pressure (Pa)	–	7.95×10^6	1.82×10^6	5.37×10^6	4.25×10^6
Stoichiometric mixture fraction (–)	0.0629	0.134	0.0627	0.100	0.0602

DME: dimethyl ether.
[a]Diesel, methanol, and n-dodecane values are given at $T = 363$ K, and DME and propane are at $T = 323$ K.

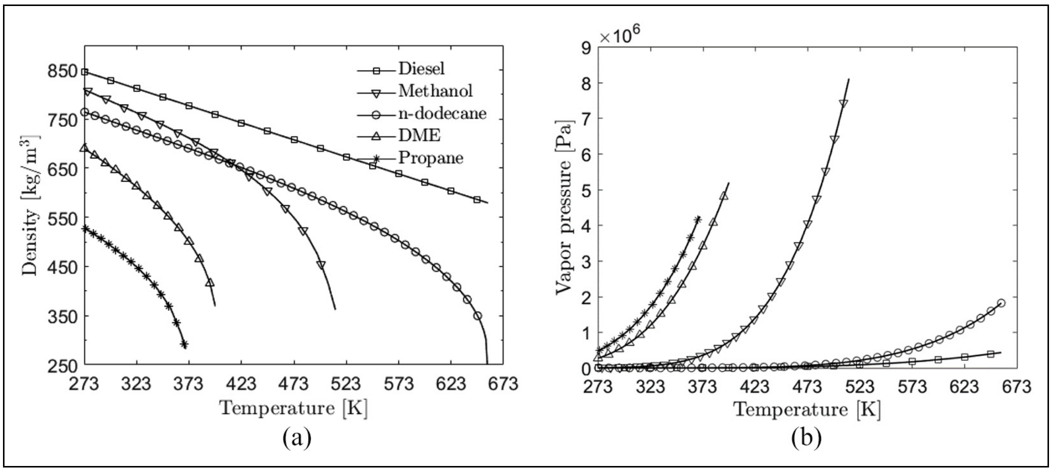

Figure 2. (a) Liquid densities and (b) vapor pressures used in the present study.

Table 4. Total injected fuel mass at $t = 1.5$ ms.

Fuels	Diesel	Methanol	*n*-dodecane	DME	Propane
Injected mass (kg)	4.00×10^{-6}	3.84×10^{-6}	3.77×10^{-6}	3.53×10^{-6}	3.02×10^{-6}

DME: dimethyl ether.

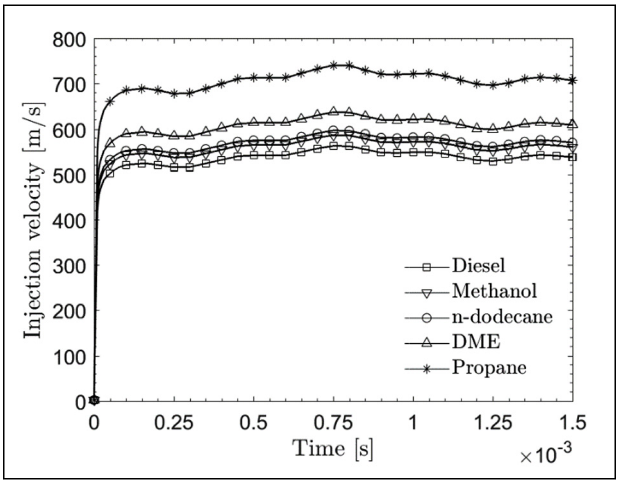

Figure 3. Injection velocity profiles for the different fuels.

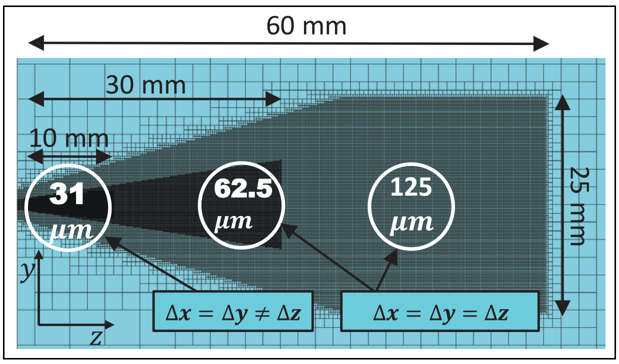

Figure 4. Computational mesh indicating local refinement areas.

The geometry of the computational domain resembles the combustion vessel at Sandia National Laboratories (the geometry of the computational domain is not exactly similar to the experimental geometry but the total volume matches that in the experiments), for which the experimental validation data are obtained. The computational domain is shown in Figure 4. Close to the nozzle exit, 31 μm cells are used in the radial directions, while in the axial direction cells are 62.5 μm long (1:2 aspect ratio). Further away from the nozzle between 10 and 30 mm (110–335D), cubical 62.5 μm cells are used. Starting from 30 mm, 125 μm cells have been utilized. Such a refinement strategy yields, altogether, 13M cells. The chosen mesh resolution is based on validation studies with different mesh resolutions in the ECN Spray A configuration.[9,11,28] These studies suggest that close to the nozzle, 62.5 μm cell size is sufficient for capturing the high gradients and mixing of vapor and surrounding air. Here, we use 31 μm cells near the nozzle in order to have better description for the shear layer dynamics and, consequently, for the fuel vapor mixing. The near-nozzle resolution is highly relevant for the observed L_{core}. A constant time step size of $dt = 5 \times 10^{-8}$ s has been used so that Co < 0.6.

Results

Spray A validation

First, the LES model is validated in the Spray A conditions using *n*-dodecane as the liquid fuel. Figure 5 shows the liquid and vapor penetrations along with the

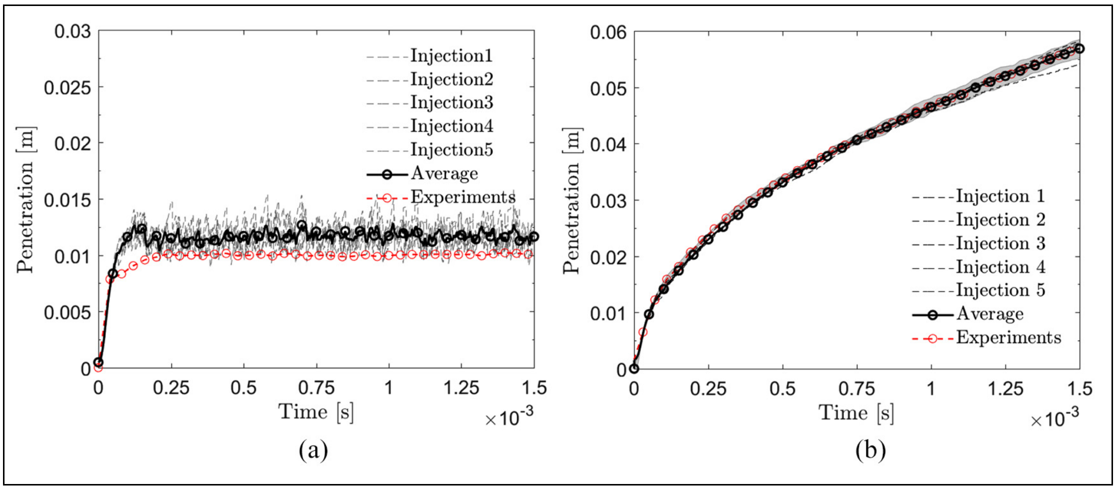

Figure 5. (a) Experimental and computational (LES) liquid length in Spray A conditions with *n*-dodecane. (b) Experimental and computational vapor penetration. The gray area indicates the experimental standard deviation.

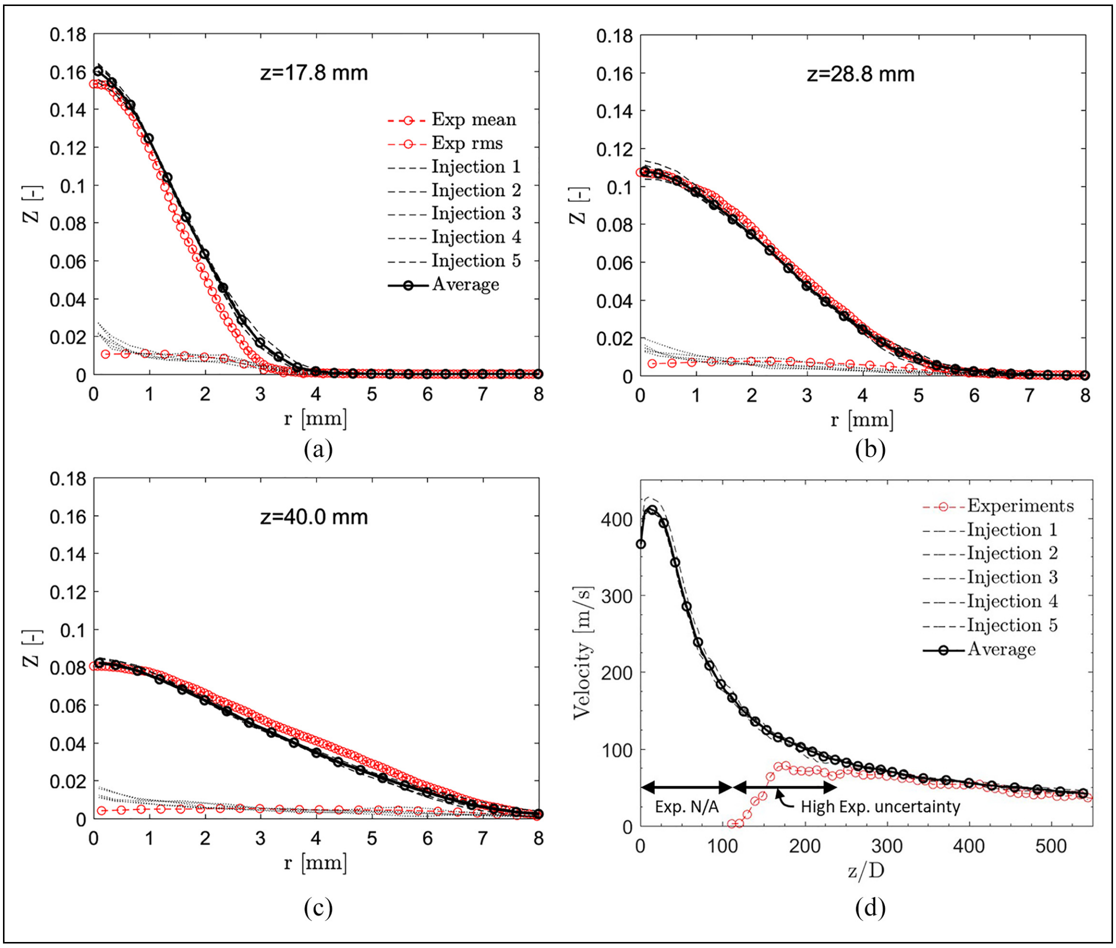

Figure 6. (a–c) Averaged radial mixture fraction (*Z*) profiles in Spray A conditions with *n*-dodecane with different distances from the nozzle. Dashed lines represent the different LES realizations. Dotted lines show the RMS for different LES realizations. (d) Mean gas phase velocity at the spray centerline.

experimental data by considering five LES realizations. The present numerical results on average liquid penetration are somewhat overestimated compared to the experimental data.[45] The average liquid length between 0.2 and 1.5 ms is 11.7 mm compared to the average experimental penetration of 10.0 mm. Here, liquid penetration is defined according to the ECN guidelines by using 0.1% liquid volume fraction for the tip penetration. The average vapor penetration is noted to match well with the experimental data.[45] Here, vapor jet tip is obtained as the axial location of 0.1% fuel vapor concentration value according to the ECN guidelines.

Figure 6 shows a comparison of the predicted radial mixture fraction profiles and experimental data.[45] The mean values are well predicted for all downstream distances. The LES result has been first circumferentially averaged and then time averaged between 1.0 and 1.5 ms for the 17.8- to 28.8-mm axial distances and between 1.3 and 1.9 ms for the 40-mm distance. Finally, ensemble average is taken between the different injections. Root mean square (RMS) values are also compared to the experimental data in Figure 6. Relatively good comparison is seen except close to the spray axis. The deviation in the RMS values is partially related to the lower statistical accuracy in spatial averaging as the number of cells decreases when approaching the spray axis.

Figure 6(d) shows the mean gas phase velocity at the spray centerline. First, the velocity increases until $z \approx 6D$ from the nozzle followed by a short spray core region (L_{core}) extending up to $z = 29D$. Further away from the nozzle (experiments valid after $z > 250D$), the predicted mean velocity closely agrees with the experimental data. The predicted mean spray centerline velocity has been time averaged between 1.3 and 1.9 ms for each injection and then ensemble averaged between the injections.

Fuel property comparison

Next, the selected five fuels (diesel, methanol, *n*-dodecane, DME, and propane) are compared with one another. For *n*-dodecane, five realizations have been computed, whereas for the other fuels, three realizations are performed. First, liquid length is analyzed between the fuels after which the evaporation, vapor penetration, and mixing characteristics are shown. Finally, the equivalence ratio fields are studied for the selected fuels.

Liquid length. Figure 7 indicates visually how an LES/LPT model performs relatively close to the nozzle. Figure 8 depicts the average spray centerline velocity for the various fuels. Several aspects related to Figures 7 and 8 can be pointed out. (1) Within the spray core length (L_{core}), droplets lose most of their momentum (for gas phase acceleration). (2) The maximum velocities within L_{core} correlate with the injection velocities of the fuels. (3) L_{core} correlates with the St number of the fuel: increased St number indicates reduced momentum transfer rate from droplets to gas phase and hence increased L_{core}. Propane has the shortest L_{core} ($L_{core} = 20D$, $St = 0.4$) followed by DME ($L_{core} = 24D$, $St = 0.5$), methanol ($L_{core} = 28D$, $St = 0.54$), *n*-dodecane ($L_{core} = 29D$, $St = 0.52$), and diesel ($L_{core} = 32D$, $St = 0.56$). (4) Efficient evaporation process starts after L_{core} due to the mixing of hot ambient gases into the spray. (5) The RMS velocities peak right after the spray core region (maximum mean velocity) and as such they consistently peak earlier for DME and propane. (6) When the centerline velocities are normalized by the peak velocities and by normalizing the axial location by L_{core}, characteristically similar gas velocity profiles are observed (see hypothesis 3).

The spray core lengths (L_{core}) have been defined as 95% of the averaged (temporally and ensemble) maximum spray centerline velocity (Figure 8). In Appendix 1, a consistency check is provided for the definition of L_{core} along with a mesh sensitivity analysis between 31, 62, and 125 µm mesh resolutions. In brief, the mesh sensitivity analysis indicates that L_{liq} is relatively unchanged for diesel, *n*-dodecane, and methanol for $dx < 125$ µm. In contrast, L_{liq} fluctuates more for DME and propane between the different meshes. For $dx < 125$ µm, $L_{liq}/L_{core} \sim 4.5$–$5$ for diesel, *n*-dodecane, and methanol, while $L_{liq}/L_{core} \sim 1.5$–$2.5$ for DME and propane. This difference can be explained by much shorter L_{liq} for DME and propane. In general, the sensitivity study indicates that with the 125-µm cell size, the definition of L_{core} is challenging due to the slow turbulence transition process. In contrast, with the 31- and 62-µm cell sizes, a consistent trend is observed

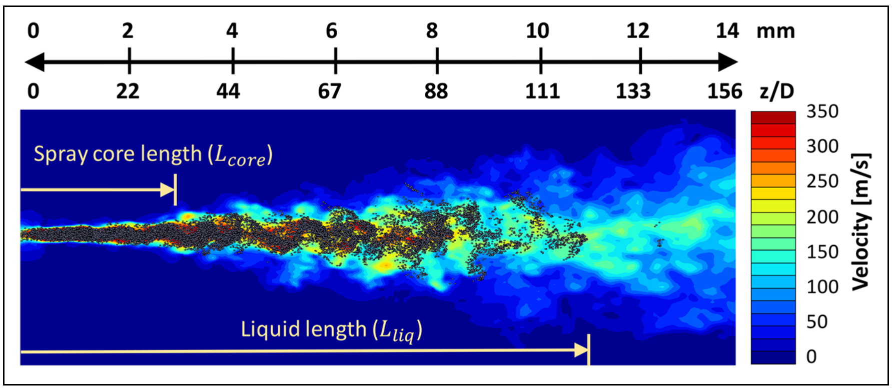

Figure 7. Near-nozzle region velocity field with droplets at $t > 1$ ms. The spray core and liquid lengths are shown.

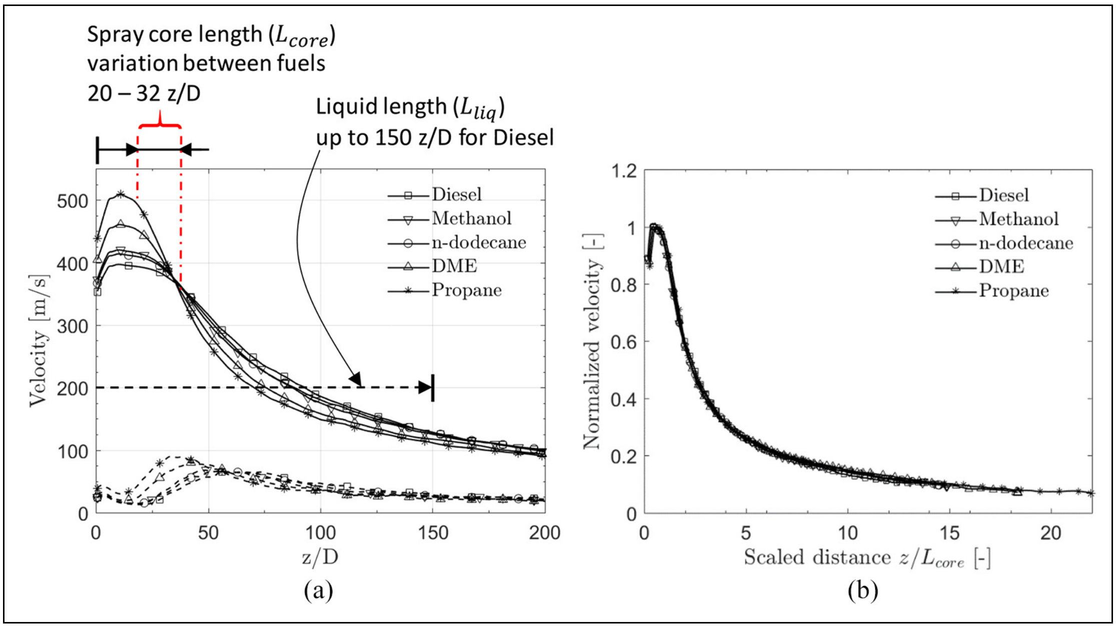

Figure 8. (a) Mean spray centerline velocity. RMS values are given with dashed lines. (b) Normalized velocity profiles indicating data collapse by normalization with peak axial velocity and L_{core}.

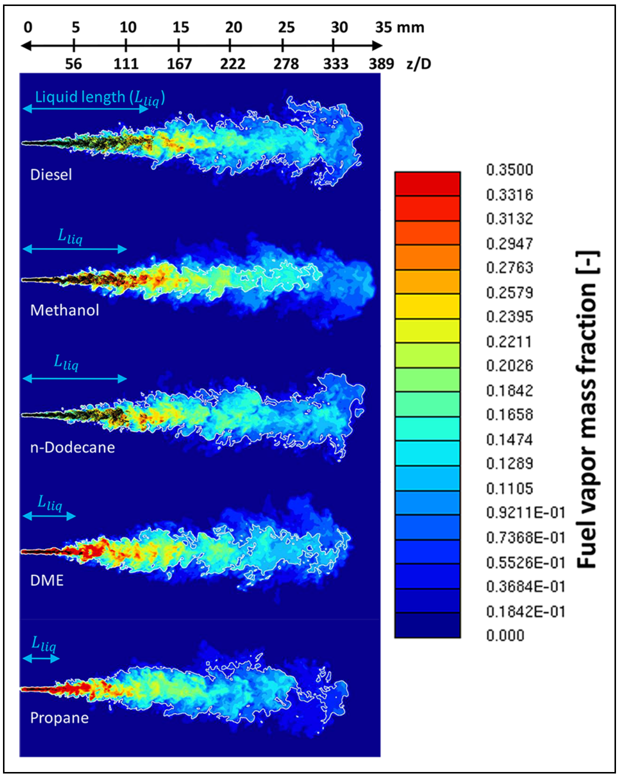

Figure 9. Fuel vapor mass fraction together with liquid droplets at $t = 0.5$ ms using 31 μm mesh density. The white line marks the $\Phi = 1$ isocontour line. L_{liq} is noted to be the longest/shortest for fuels with the longest/shortest L_{core}.

where L_{core} either stays constant or increases with increasing cell size.

Figure 9 shows the fuel concentration fields together with droplets at $t = 0.5$ ms. Large differences are observed in the liquid part of the sprays between the "long liquid length" fuels (diesel, *n*-dodecane, and methanol) and the "short liquid length" fuels (DME and propane). The relatively long liquid penetration of methanol is somewhat unexpected based on its vapor pressure curve (Figure 2(b)). However, this is related to the high latent heat of methanol that lowers the gas phase temperature during evaporation (see Figure 15).[13] It is worth noting that the stoichiometric isoline may deviate considerably within the spray envelope depending on the fuel. While the $\Phi = 1$ contour locates on the outer shell of the spray in the diesel case, for methanol, the stoichiometric conditions are found only at the core of the spray. Such a feature should be considered, when ignition and quasi-steady flame lift-off length estimates are constructed without detailed simulations.

Figure 10(a) illustrates the obtained liquid lengths for the various fuels. The variation in the average liquid length (0.2–1.5 ms) between different LES realizations was less than 2% for all fuels. With relevance to the obtained spray core lengths for the fuels (Figure 8), Figure 10(b) correlates L_{core} to liquid density. It is seen that higher liquid density implies higher L_{core}. This result is related to the increasing St number with fuel density ($St \sim \rho_f$). As already indicated, increased St number indicates reduced momentum transfer rate from droplets to gas phase and hence increased L_{core}.

Figure 11(a) indicates a positive correlation between the fuel density and the average liquid length. The

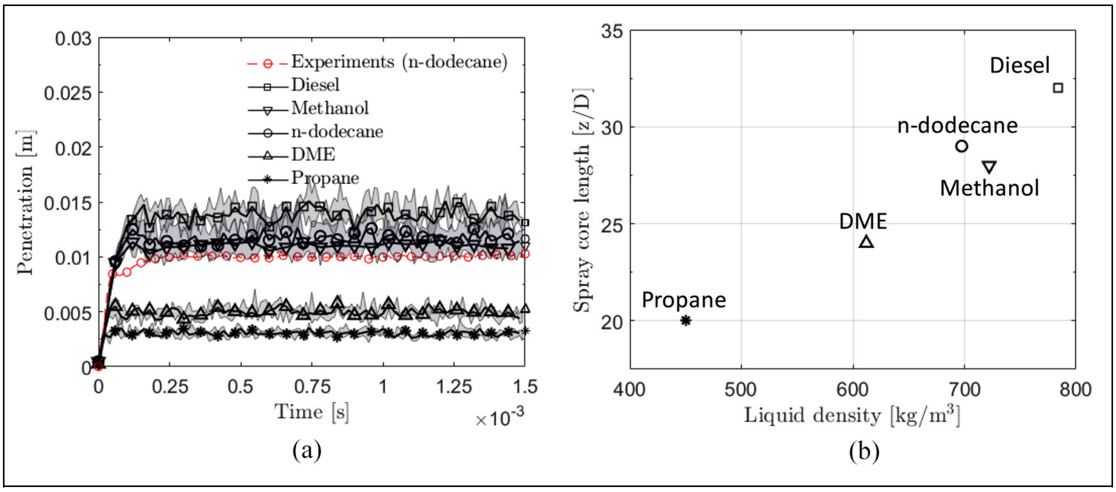

Figure 10. (a) Average liquid penetration. The shaded areas represent minimum/maximum values from different LES realizations. (b) The effect of liquid density on the spray core length (L_{core}). The result can be explained by the relationship $\rho_f \sim St$ and increased L_I with St.

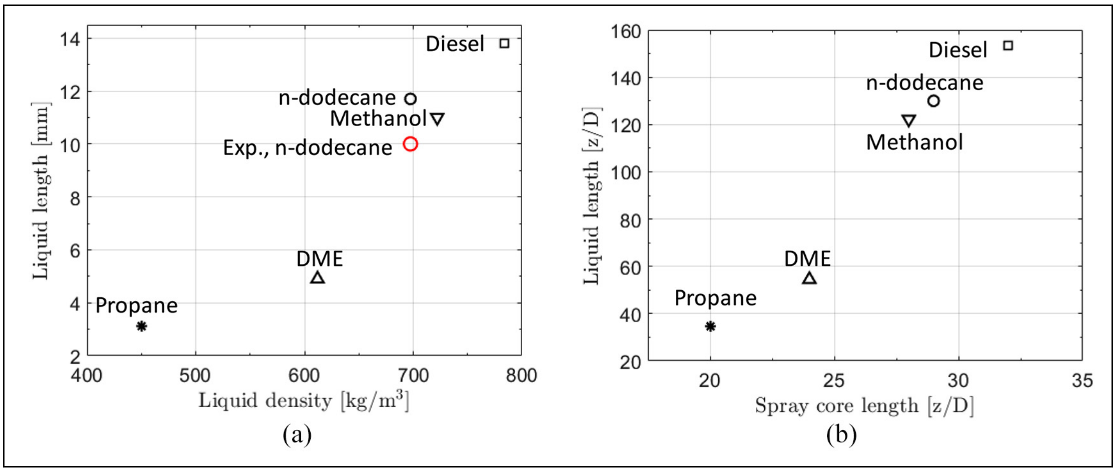

Figure 11. (a) Effect of fuel density on liquid length (L_{liq}). A higher fuel density leads to increased L_I, L_{II}, L_{core}, and L_{liq}. (b) The effect of spray core length (L_{core}) on L_{liq}. For all the fuels, L_{liq} is longer than L_{core}, confirming the increased mixing of hot air into the spray after L_{core}.

observation is qualitatively in line with the experimental results by Kook and Pickett[22] and Naber and Siebers.[46] Based on the classical understanding, the entrained ambient mass ($\dot{m}_a$) per fuel mass ($\dot{m}_f$) is inversely proportional to fuel density according to $\dot{m}_a/\dot{m}_f \sim \sqrt{(\rho_a/\rho_f)}(\tan(\Theta)/D)z$, where z is the axial distance from the nozzle and Θ is the spray angle.[46] Thereby, a higher fuel density decreases $\dot{m}_a/\dot{m}_f$ leading to a longer liquid length when ambient entrainment (mixing) limited vaporization is assumed. The scaling law by Siebers[14] indicates liquid length dependence on fuel–air density ratio as $L_{liq} \sim \sqrt{\rho_f/\rho_a}$. However, under-resolved near-nozzle LES/LPT simulations do not necessarily capture such scaling. Indeed, in contrast to the square-root behavior, here we observe more likely a linear scaling. In addition to resolution aspects, the deviation can be explained by the much lower density ratio range used in the present study $20 < \rho_f/\rho_a < 34$ compared to that used by Siebers[14] $13 < \rho_f/\rho_a < 220$. Based on the present numerical results, a higher fuel density leads to increased L_I, L_{II}, L_{core}, and L_{liq}. In the present model, L_I is solely dependent on St which further affects L_{II}, L_{core}, and L_{liq}. Thereby, consistent with Siebers et al.,[14] the higher the density, the longer the L_{liq}. However, the new LES/LPT-specific aspect here is the intertwined character of the four length scales which emerge from St.

With relevance to hypothesis 1, Figure 11(b) shows the correlation between L_{core} and L_{liq}. It is noted that

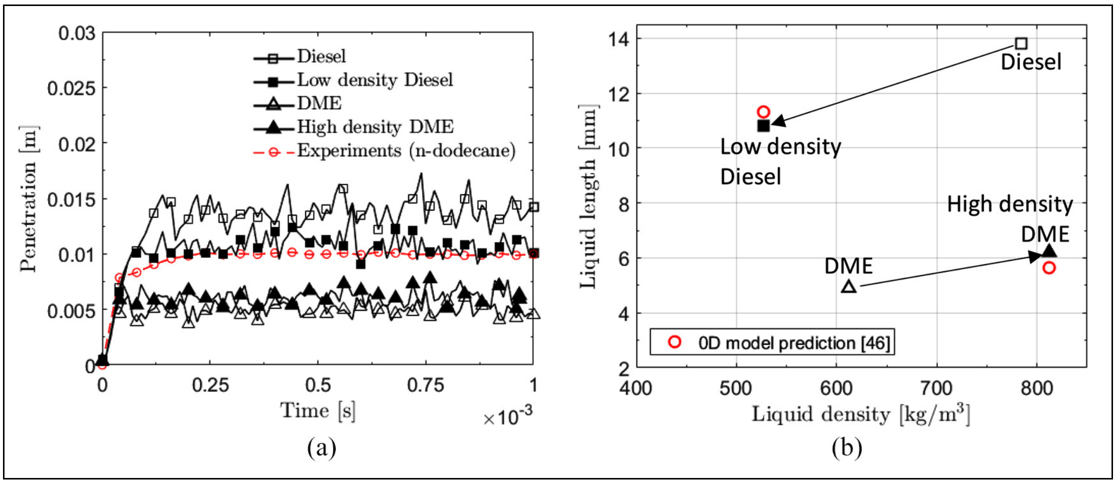

Figure 12. (a) Liquid penetration with modified liquid density. (b) Effect of changing liquid density on diesel and DME liquid length. Red symbols indicate a model prediction by Naber and Siebers.[46]

L_{liq} is always larger than L_{core} confirming hypothesis 1. Since droplet evaporation is weak within L_{core} due to low entrainment, it is expected that $L_{liq} > L_{core}$. In particular, a linear fit to the data indicates that $L_{liq} = 10.8L_{core} - 189$ $[z/D]$. Thereby, in the present model setup, the spray core length has a significant effect on the liquid length. The liquid lengths in Figure 11(a) and (b) have been time averaged between 0.2 and 1.5 ms.

A numerical test on virtual fuels. According to Kook and Pickett,[22] the effect of liquid density on liquid length is not fully understood. In general, assessing this in experiments is challenging as the density and other properties of fuels are typically interlinked. On the other hand, in numerical simulations it is possible to assess variation in only a specific quantity. The idea here is to emulate a virtual diesel and DME in order to quantify the sole effect of density on the liquid length.

Next, such a virtual fuel test is used to assess the liquid density effect on liquid length. Two test cases are carried out. In the first case, diesel liquid density was scaled down to that of DME ("low density diesel"). All other properties were as in the original diesel fuel. In the second case, liquid density of DME was scaled up to that of diesel ("high density DME"). Again, all other properties were as in the original DME fuel. Obviously, consistent with the endeavor to maintain a constant injection pressure, the density changes affected the resulting injection velocity according to $\Delta U_{inj} \sim \sqrt{\rho_1/\rho_2}$, where subscript 1 refers to the original liquid density and 2 to the new density.

Figure 12(a) shows the resulting liquid length as a function of time, while Figure 12(b) indicates the effect of liquid density on the average liquid length. A positive correlation is observed between L_{liq} and density, as already noted in Figure 11. However, it is observed that the "low density diesel" does not have the liquid length

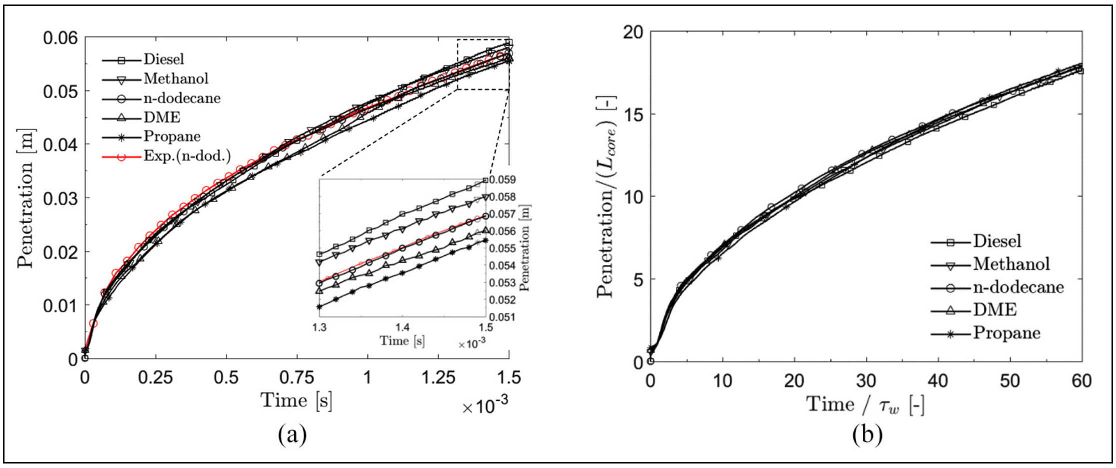

Figure 13. (a) Ensemble-averaged vapor penetration for the different fuels. It is observed that the vapor penetrations increase with higher L_{core}. (b) Scaled vapor penetration for the different fuels showing similarity between the penetrations after L_{core}.

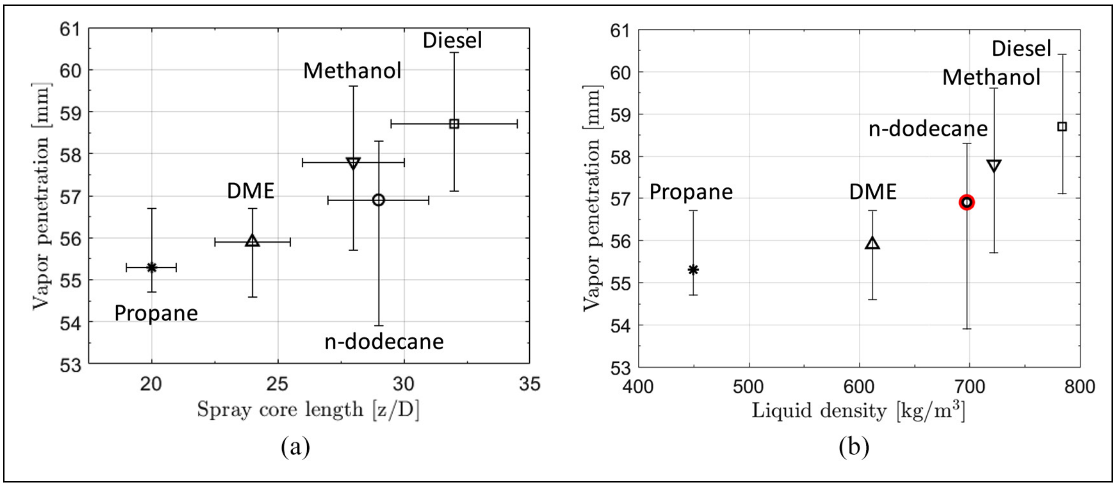

Figure 14. (a) Effect of spray core length (L_{core}) on vapor penetration (L_{vap}) at $t = 1.5$ ms. It is noted that the maximum vapor penetration correlates with L_{core}. (b) Effect of fuel density on L_{vap}. Increased density indicates higher St yielding higher L_l, L_{ll}, L_{core}, and L_{vap}. Vertical error bars show the variation between different LES realizations. Red circle marks the experimental value.

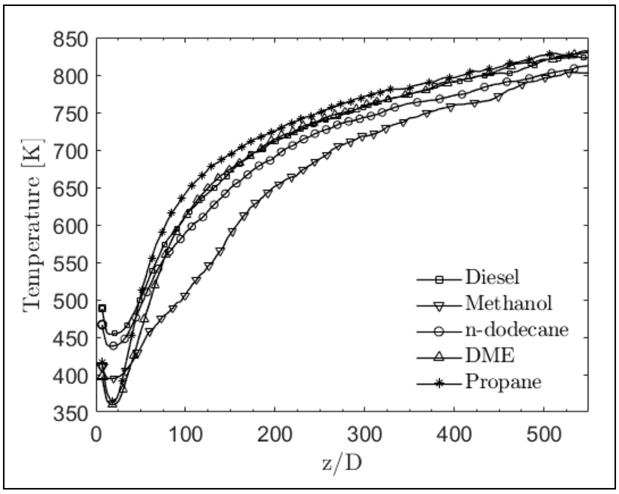

Figure 15. Mean gas phase temperature at the spray centerline. Rapid temperature increase is noted after L_{core} while methanol exhibits the strongest cooling effect of the ambient gas.

of DME, nor does the "high density DME" have the liquid length of diesel. In fact, the change in liquid length only accounts between 15% and 33% of the difference between the liquid length of diesel and DME. The implication is that other properties, such as vapor pressure and boiling point, play a more significant role in defining the liquid length of a fuel (hypothesis 2). This is consistent with various previous observations.[20–22] In addition, the importance of vapor pressure for the evaporation process can also be noted from equation (13). The accuracy of the zero-dimensional (0D) model by Naber and Siebers[46] is noted to be within 10% in predicting the liquid length correctly. This can be considered to be a relatively good agreement since the changes in density were rather significant.

Evaporation and mixing. Next, we analyze the differences in evaporation and mixing between the fuels. The analysis is started by considering vapor jet penetrations with focus on proper normalization. It is of particular interest to find a similarity relationship between the different fuels. Figure 13(a) illustrates the average penetrations for the fuels. It is noted that the higher the L_{core}, the higher the final vapor penetration at $t = 1.5$ ms. In Figure 13(b), the vapor penetration has been scaled with L_{core}. Time has been normalized with $\tau_w = W/U_L$, where W is the spray width and U_L is the axial velocity at L_{core}. Hence, the vapor penetrations of the various fuels are seen to scale with their respective spray core values. Similarly, in conventional gas-jet studies, a self-similar solution is obtained by normalizing the statistics by the steady potential core, that is, virtual origin.[30] Importantly, related to hypothesis 3, L_{core} seems to have a governing role in the final vapor jet penetration. Within the spray core, the droplet laden jet velocity is faster compared to the situation after the spray core (Figure 8). Thereby, the longer the spray core length, the greater the distance from the nozzle where the mixing-induced slower velocity region starts. When considering the absolute vapor jet penetrations between the fuels, Figure 14(a) indicates a positive correlation between the L_{core} and the L_{vap}. However, we note that the trend remains relatively weak.

Earlier, it has been proposed that vapor penetration would not be related to liquid density.[22] The argument is that the fuel spray momentum flux $\dot{M} \sim \Delta p A_D$ is not dependent on liquid density. However, the average vapor penetrations in Figure 14(b) are noted to be positively correlated with liquid density. This observation is not fully in line with the experimental findings in Kook and Pickett[22] which were based on a more narrow liquid density range (755–870 kg/m^3) compared to the present study. Similar to Figure 14(a), the correlation

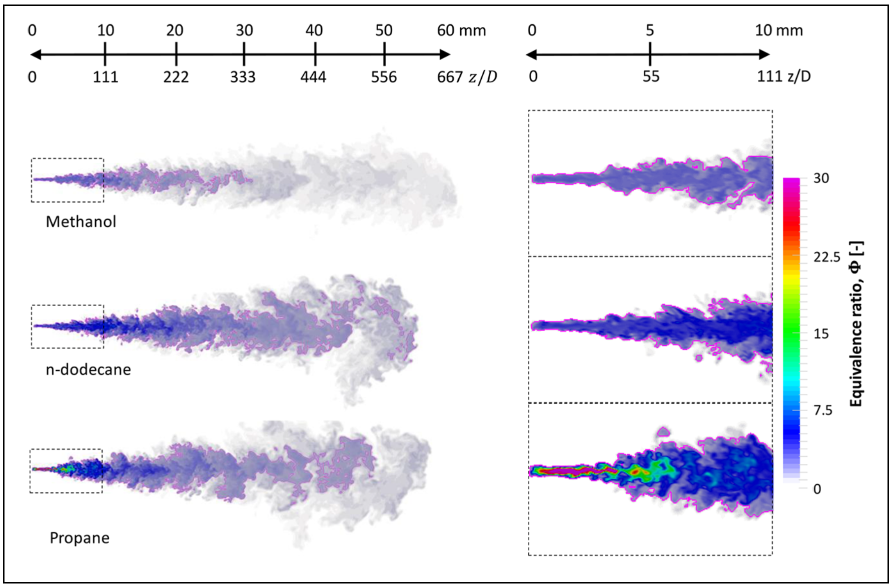

Figure 16. Equivalence ratio (Φ) fields at $t = 1.5$ ms. The red line marks the $\Phi = 1$ isocontour line. A zoom to the near-nozzle region (dashed boxes) is shown on the right-hand side column.

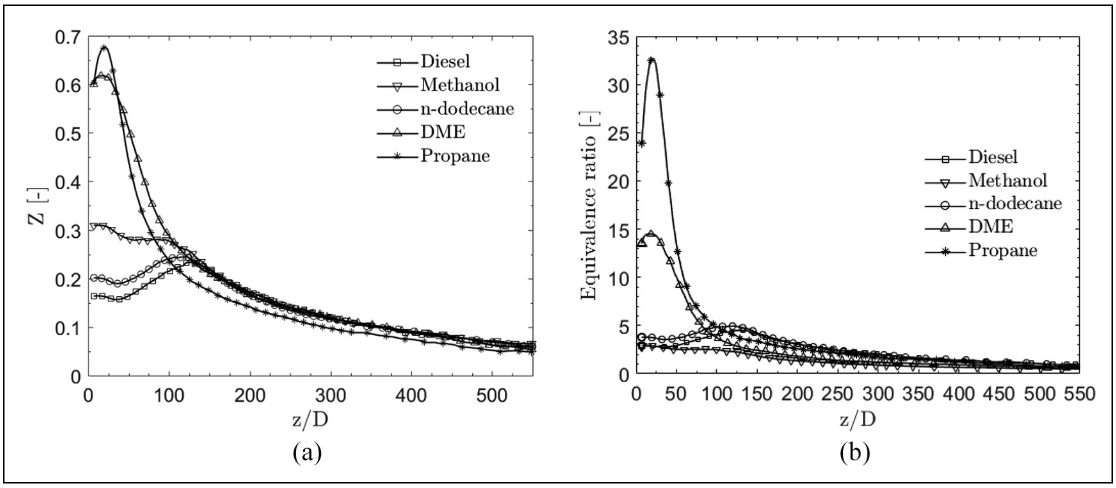

Figure 17. (a) Mean spray centerline mixture fraction for the fuels. Near-nozzle differences are noted to be high, while, further away from the nozzle, the profiles collapse with propane as an exception. (b) Mean spray centerline equivalence ratio (Φ) Methanol has the lowest Φ from the injector up to the vapor tip, while DME has the second lowest Φ after $z \approx 100D$.

found here is relatively weak. It is also noted that the injection-to-injection fluctuations are higher for the vapor penetration ($< 4\%$) than for the liquid length ($< 2\%$) as expected.

Figure 15 illustrates the mean spray centerline temperature of the gaseous phase. The low local temperatures close to the nozzle are noted to be approximately 450–550 K lower than the average gas phase temperature of 900 K. The lowest near-nozzle temperatures are observed with DME and propane. This is due to their very fast evaporation rate leading to a rich and cool mixture which is consistent with Figure 9 as well. Apart from the near-nozzle region, the very high latent heat of methanol is clearly seen as lower centerline temperature compared to the other fuels. Right after the liquid length ($z > 125D$), methanol has 70–130 K lower gas phase temperature compared to the other fuels. *n*-dodecane has the second highest latent heat which is reflected in equivalent centerline temperature. The low heat of evaporation of propane and low fuel concentration after the near-nozzle region is noted to result as the highest gas phase temperature.

Equivalence ratio. Next, we examine the equivalence ratio (Φ) fields of the five fuels. Figure 16 shows the equivalence ratios from the spray centerline cross-section at $t = 1.5$ ms. The broad range of Φ values is clearly visible as propane has maximum $\Phi > 30$, DME has maximum $\Phi \sim 15$, while diesel, methanol, and *n*-dodecane have much lower maximum values $\Phi < 6$. The trends for DME and diesel are not shown here for brevity. In addition, it is interesting to look at the axial extent of the rich mixture region, here marked with $\Phi = 1$ iso-contour line, because it could potentially influence the combustion process of these fuels. For example, it has been observed that high temperature ignition, for typical liquid fuels, takes place between $1 < \Phi < 2$.[12] For *n*-dodecane and diesel, the rich mixture area extends up to the vapor tip region of the gas jet. Interestingly, almost the same situation is seen for propane. The fuels containing oxygen, DME, and methanol have much shorter rich mixture penetration length.

Figure 17(a) shows the mean spray centerline mixture fraction, while Figure 17(b) presents the mean spray centerline equivalence ratio. Very high Φ values are noted close to the nozzle for DME and propane. This is related to their high vaporization rates. Diesel and *n*-dodecane have a second peak close to their L_{liq} ($z \sim 125D$). Methanol has the lowest Φ all the way starting from the injector up to the vapor tip, while DME has the second lowest Φ after $z \approx 100D$. These differences could potentially have significant effect on combusting sprays, such as ignition phenomena, flame lift-off length (FLOL), or soot formation.[47,48]

Conclusion

Here, diesel, methanol, *n*-dodecane, DME, and propane sprays were numerically compared using LES/LPT. The numerical setup was based on the ECN Spray A target conditions and the fuel was changed by keeping the injection pressure constant. As an obvious consequence, the injection velocity and fuel mass flow rates were affected. The modeling work presented here targets (1) to yield insight for modelers encountering complex spray cases with various fuels in their daily practices and (2) to provide a basis for potential experimental work on such fuel comparison. First, the LES/LPT model was validated in the ECN Spray A target condition with *n*-dodecane. Second, fuel comparison was carried out focusing mostly on the liquid lengths as well as on the vapor penetrations between the different fuels. The fuel–air mixing and the resulting equivalence ratio fields were also studied due to their paramount importance to, for example, emission formation under reacting conditions. Finally, also the injection-to-injection effects were analyzed. The main conclusions of the present study can be summarized as follows:

1. With relevance to hypothesis 1, a strong link between liquid length (L_{liq}) and spray core length (L_{core}) was confirmed to exist in the present numerical model according to $L_{liq} = 10.8L_{core} - 189$ $[z/D]$. In addition, L_{liq} was shown to be positively correlated with liquid density consistent with previous studies.
2. A separate sensitivity test on virtual diesel and DME revealed that the virtual diesel with DME density did not yield the DME L_{liq}. Thereby, only a relatively weak dependency between the liquid density and L_{liq} was observed. At maximum, 33% of the observed differences in L_{liq} could be explained by the liquid density. This implies that thermodynamics plays a more important role in spray evaporation than density.
3. Vapor jet penetration (L_{vap}) was noticed to scale with L_{core} according to $L_{vap}/L_{core} = A\sqrt{(t/\tau_w)}$, where A = 2.37 confirming hypothesis 3. Therefore, the vapor jet tip penetrations were similar between the fuels in non-dimensional form.
4. The evaporative cooling effect of various fuels at the spray centerline is shown here for the first time. The local gas phase temperature for methanol was noted to be 70–130 K lower compared to the other fuels.
5. The study revealed significant differences in the local equivalence ratio fields for the fuels. Diesel, *n*-dodecane, and propane exhibited relatively similar equivalence ratio fields after the near-nozzle region. In contrast, DME and methanol showed much lower average equivalence ratios within the mixture.
6. Injection-to-injection variations were observed, and the variations were lower for liquid length ($< 2\%$) compared to vapor penetration ($< 4\%$). Fuels with longer vapor penetration/liquid length (diesel, *n*-dodecane, and propane) had also higher variation in vapor penetration /liquid length.

It should be noted that the present results are of numerical character. The discussed length scales are clearly linked to one another, but the relationship is inherently dependent on (1) near-nozzle modeling assumptions and (2) grid resolution. We note that presently very little is known on near-nozzle gas and liquid velocities. Here, an attempt was made to shed light on certain features of LES/LPT spray models. The present numerical model explains consistently the trends in fuel property variation for all the fuels. Based on the study, we note that experimental evidence of axial velocity profiles for $z/D < 250$ would be highly valuable for various fuels.

Declaration of conflicting interests

The author(s) declared no potential conflicts of interest with respect to the research, authorship, and/or publication of this article.

Funding

The author(s) disclosed receipt of the following financial support for the research, authorship, and/or publication of this article: This work was supported by the European Union HERCULES-2 project within Horizon 2020 research and innovation program under grant agreement no. 634135. The present study has also been financially supported by the Academy of Finland (grant nos 289592 and 318024) and by the King Abdullah University of Science and Technology, Office of Sponsored Research (OSR) under Award OSR-2017-3319. The simulations presented above were performed using computer resources within the Aalto University School of Science "Science-IT" project.

ORCID iDs

Ossi Tapani Kaario https://orcid.org/0000-0001-6765-0807
Heikki Kahila https://orcid.org/0000-0002-4103-7833

References

1. Engine Combustion Network Workshop 4, 2015, http://www.sandia.gov/ecn/workshop/ECN4/ECN4.php
2. Pickett L, Genzale C, Bruneaux G, Malbec L, Hermant L, Christiansen C, et al. Comparison of diesel spray combustion in different high-temperature, high-pressure facilities. *SAE Int J Engines* 2010; 3(2): 156–181.
3. Bhattacharjee S and Haworth DC. Simulations of transient n-heptane and n-dodecane spray flames under engine-relevant conditions using a transported PDF method. *Combust Flame* 2013; 160(10): 2083–2102.
4. Pei Y, Hawkes ER, Kook S, Goldin GM and Lu T. Modelling n-dodecane spray and combustion with the transported probability density function method. *Combust Flame* 2015; 162(5): 2006–2019.
5. Xue Q, Battistoni M, Powell CF, Longman DE, Quan SP, Pomraning E, et al. An Eulerian CFD model and X-ray radiography for coupled nozzle flow and spray in internal combustion engines. *Int J Multiphase Flow* 2015; 70: 77–88.
6. Blomberg C, Zeugin L, Pandurangi S, Bolla M, Boulouchos K and Wright Y. Modeling split injections of ECN "Spray A" using a conditional moment closure combustion model with RANS and LES. *SAE Int J Engines* 2016; 9(4): 2107–2119.
7. Xue Q, Som S, Senecal PK and Pomraning E. Large eddy simulation of fuel-spray under non-reacting IC engine conditions. *Atom Spray* 2013; 10: 925–955.
8. Irannejad A and Jaberi F. Numerical study of high speed evaporating sprays. *Int J Multiphase Flow* 2015; 70: 58–76.
9. Gong C, Jangi M, Lucchini T, D'Errico G and Bai XS. Large Eddy simulation of air entrainment and mixing in reacting and non-reacting diesel sprays. *Flow Turbulence Combust* 2014; 93(3): 385–404.
10. Pei Y, Som S, Pomraning E, Senecal PK, Skeen SA, Manin J, et al. Large eddy simulation of a reacting spray flame with multiple realizations under compression ignition engine conditions. *Combust Flame* 2015; 162(12): 4442–4455.
11. Wehrfritz A, Kaario O, Vuorinen V and Somers B. Large Eddy simulation of n-dodecane spray flames using flamelet generated manifolds. *Combust Flame* 2016; 167: 113–131.
12. Kahila H, Wehrfritz A, Kaario O, Ghaderi Masouleh M, Maes N, Somers B, et al. Large-Eddy simulation on the influence of injection pressure in reacting spray A. *Combust Flame* 2018; 191: 142–159.
13. Higgins BS, Mueller CJ and Siebers DL. Measurements of fuel effects on liquid-phase penetration in DI sprays. *SAE Trans J Engines* 1999; 108(3): 630–643.
14. Siebers DL. Scaling liquid-phase fuel penetration in diesel sprays based on mixing-limited vaporization. SAE Technical paper 1999-01-0528, 1999.
15. Stanton DW, Lippert AM, Reitz RD and Rutland CJ. Influence of spray-wall interaction and fuel films on cold starting in direct injection diesel engines. *SAE Trans J Fuels Lubric* 1998; 107: 1540–1563.
16. Hulkkonen T, Tilli A, Kaario O, Ranta O, Sarjovaara T, Vuorinen V, et al. Late post-injection of biofuel blends in an optical diesel engine: experimental and theoretical discussion on the inevitable wall wetting effects on oil dilution. *Int J Engine Res* 2017; 18(7): 645–656.
17. Genzale CL, Pickett LM and Kook S. Liquid penetration of diesel biodiesel sprays at late-cycle post-injection conditions. *SAE Int J Engines* 2010; 3: 479–495.
18. Tilli A, Hulkkonen T, Kaario O, Larmi M, Sarjovaara T and Lehto K. Biofuel blend late post-injection effects on oil dilution and diesel oxidation catalyst performance. *Int J Engine Res* 2017; 19: 941–951.
19. Crowe CT, Schwarzkof JD, Sommerfeld M and Tsuji Y. *Multiphase Flows with Droplets and Particles*. 2nd ed. Boca Raton, FL: CRC Press, 2012.
20. Canaan RE, Dec JE, Green RM and Daly DT. The influence of fuel volatility on the liquid-phase fuel penetration in a heavy-duty D.I.diesel engine. SAE Technical paper 980510, 1998.
21. Siebers DL. Liquid-phase fuel penetration in diesel sprays. *SAE Technical paper* 980809, 1998.
22. Kook S and Pickett LM. Liquid length and vapor penetration of conventional, Fischer-Tropsch, coal-derived, and surrogate fuel sprays at high-temperature and high-pressure ambient conditions. *Fuel* 2012; 93: 539–548.
23. Yu H, Goldsworthy L, Ghiji M, Brandner PA and Garaniya V. A parallel volume of fluid-Lagrangian Parcel Tracking coupling procedure for diesel spray modeling. *Comp Fluids* 2017; 150: 46–65.
24. Aggarval AK, Som S, Shukla PC, Goyal H and Longman D. In-nozzle flow and spray characteristics for mineral diesel, Karanja, and Jatropha biodiesels. *Appl Energ* 2015; 156: 138–148.
25. Torelli R, Som S, Pei Y, Zhang Y and Traver M. Influence of fuel properties on internal nozzle flow development in a multi-hole diesel injector. *Fuel* 2017; 204: 171–184.
26. Som S, Longman DE, Ramirez AI and Aggarwal SK. A comparison of injector flow and spray characteristics of biodiesel with petrodiesel. *Fuel* 2010; 89: 4014–4024.
27. Som S and Longman DE. Numerical study comparing the combustion and emission characteristics of biodiesel to petrodiesel. *Energ Fuel* 2011; 25: 1373–1386.
28. Wehrfritz A, Vuorinen V, Kaario O and Larmi M. Large Eddy simulation of high velocity fuel sprays: studying mesh resolution and breakup model effects for spray A. *Atom Spray* 2013; 23(5): 419–442.
29. Kaario O, Vuorinen V, Hulkkonen T, Keskinen M and Larmi Ma Tanner F. Large Eddy simulation of high gas density effects in fuel sprays. *Atom Spray* 2013; 234: 297–325.
30. Boersma BJ, Brethouwer G and Nieuwstadt FTM. A numerical investigation on the effect of the inflow

conditions on the self-similar region of a round jet. *Phys Fluid* 1998; 10(4): 899.
31. Sutherland WLII. The viscosity of gases and molecular force. *Philosophical Magazine Series* 1893; 536: 223, 507–531.
32. Speziale CG. Analytical methods for the development of Reynolds-stress closures in turbulence. *Ann Rev Fluid Mech* 1991; 23: 107–157.
33. Sone K and Menon S. Effect of subgrid modeling on the in-cylinder unsteady mixing process in a direct injection engine. *J Eng Gas Turb Power* 2003; 125: 435–443.
34. CD-Adapco Methodology STAR-CD version 4. 24, 2015.
35. Bode M, Davidovic M and Pitsch H. Multi-scale coupling for predictive injector simulations. New York: Springer, 2017.
36. Kastengren A, Ilavsky J, Juan Pablo Viera Payri R, Duke DJ, Swantek A, Tilocco FZ, et al. Measurements of droplet size in shear-driven atomization using ultra-small angle x-ray scattering. *Int J Multiphase Flow* 2017; 92: 131–139.
37. Kaario O, Vuorinen V, Zhu L, Larmi M and Liu R. Mixing and evaporation analysis of a high-pressure SCR system using a hybrid LES-RANS approach. *Energy* 2017; 120: 827–841.
38. Bird RB, Stewart EW and Lightfoot EN. *Transport Phenomena*. New York: John Wiley Sons, 1966.
39. Ranz WE and Marshall WR. Evaporation from drops—parts I and II. *Chem Eng Prog* 1952; 48(3): 141.
40. *Utilization of Diesel Oil in Combustion Applications (Öljyn käyttö kattilalaitoksissa)*. Shanghai, China: Neste ltd, 1991.
41. Murphy MJ and Lanning LA. Vapor pressures of diesel fuel oxygenate blends. SAE paper 2002-01-2850, 2002.
42. Teng H, McCandless JC and Schneyer JB. Thermodynamic properties of dimethyl ether—An alternative fuel for compression-ignition engines. SAE paper 2004-01-0093, 2004.
43. Linstrom PJ and Mallard WG (eds). *NIST Chemistry WebBook, NIST Standard Reference Database Number 69, National Institute of Standards and Technology*. Gaithersburg, MD: NIST.
44. Ainsalo A, Sallinen R, Kaario O and Larmi M. Optical investigation of spray characteristics for light fuel oil, kerosene, hexane, methanol, and propane. *Atom Spray*, in press.
45. Pickett L, Manin J, Genzale C, Siebers D, Musculus M and Idicheria C. Relationship between diesel fuel spray vapor penetration/dispersion and local fuel mixture fraction. *SAE Int J Engines* 2011; 4(1): 764–799.
46. Naber JD and Siebers DL. Effects of gas density and vaporization on penetration and dispersion of diesel sprays. *SAE Trans J Engines* 1996; 105: 82–111.
47. Maes N, Meijer M, Dam N, Somers B, Toda HB, Bruneaux G, et al. Characterization of spray A flame structure for parametric variations in ECN constant-volume vessels using chemiluminescence and laser-induced fluorescence. *Combust Flame* 2015; 35: 3167–3174.
48. Skeen S, Manin J and Pickett LM. Simultaneous formaldehyde PLIF and high-speed Schlieren imaging for ignition visualization in high-pressure spray flames. *Proc Combust Inst* 2015; 35: 3167–3174.

Appendix 1

Mesh sensitivity analysis

The purpose of the appendix is twofold: (1) to assess the definition of L_{core} and (2) to carry out a mesh sensitivity analysis. The spray core length is defined from the time-averaged spray centerline velocity. The time averaging has been carried out between 1.3 and 1.9 ms. The resolutions in the near-nozzle region are (see Figure 4) as follows: 31, 62, and 125 μm. Figure 18 shows the averaged maximum spray centerline velocities for the tested five fuels for three mesh resolutions. The peak velocity decrease for finer grids can be explained with enhanced radial momentum generation.

Figure 19(a) shows the effect of mesh density on L_{liq}/L_{core}, while Figure 19(b) depicts the effect of mesh resolution on L_{liq}. It is noted that the fuels are divided into two different groups: (1) diesel, *n*-dodecane, and methanol and (2) DME and propane. We note that group 1 includes fuels with low vapor pressure and high initial temperature. In contrast, group 2 includes fuels with high vapor pressure and lower initial temperature. In general, $L_{liq} > L_{core}$ which is consistent with hypothesis 1. For group 1, the considered metrics are practically unchanged below 125 μm. For group 2, more variation is noted due to low boiling point effects. Tables 5 and 6 show the obtained and values. For $dx < 125\,\mu m$, $L_{liq}/L_{core} \sim 4.5$–5 for group 1, while $L_{liq}/L_{core} \sim 1.5$–2.5 for group 2. As a remark, we have also carried out a sensitivity check for two alternative definitions on the spray core length based on either 90% or 95% of the averaged maximum spray centerline velocity. It is observed that these definitions yield similar and consistent trends (see Table 5). In conclusion, the analysis indicates that $L_{liq} \sim L_{core}$ for $dx < 125\,\mu m$ in the present Large-Eddy simulation (LES)/Lagrangian particle tracking (LPT) model. Hence, hypotheses 1, 2, and 3 seem to hold for the present model.

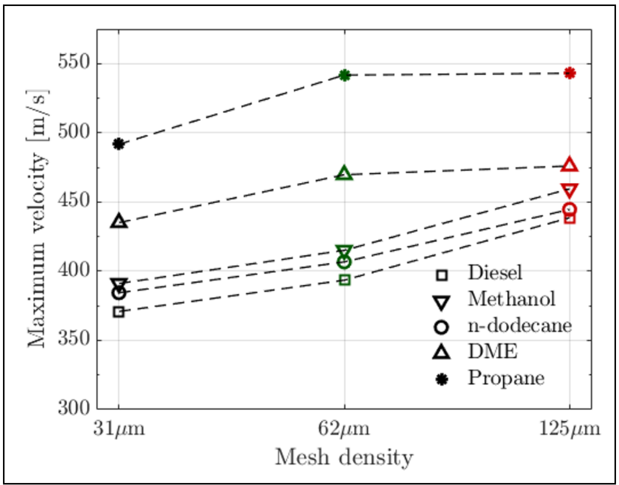

Figure 18. Effect of mesh resolution on the averaged maximum spray centerline gas phase velocity. Black marker represents the 31-μm mesh, green marker the 62-μm mesh, and red marker the 125-μm mesh.

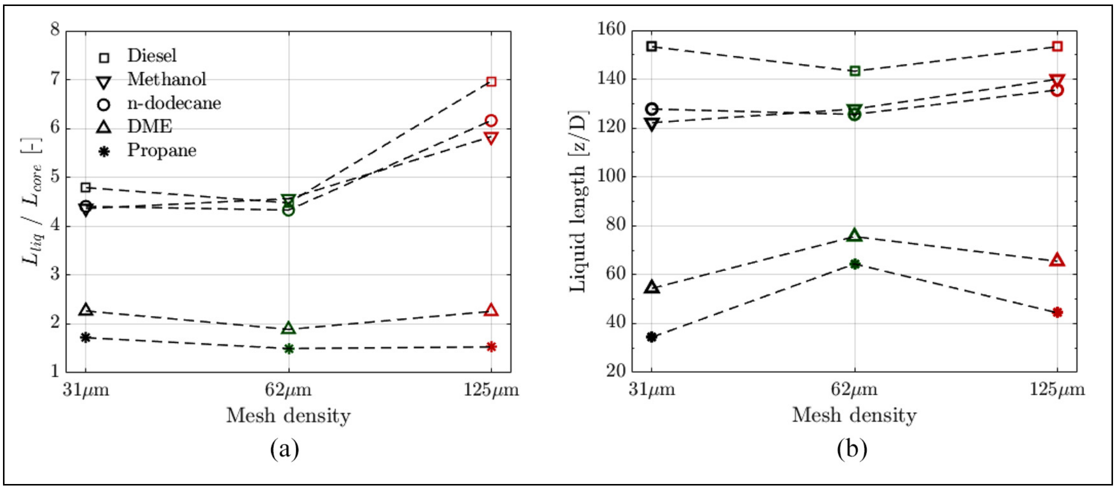

Figure 19. (a) Effect of mesh density on L_{liq}/L_{core}. (b) Mesh comparison of L_{liq}.

Table 5. Spray core (L_{core}) [z/D] as a function of mesh density and 90%/95% U_{max} definition.

	L_{core}, 95% U_{max}			L_{core}, 90% U_{max}		
Mesh/smallest cell size	31 μm	62 μm	125 μm	31 μm	62 μm	125 μm
Diesel	32	32	22	38	39	33
Methanol	28	28	24	33	39	38
n-dodecane	29	29	22	35	36	33
DME	24	40	29	28	49	49
Propane	20	43	29	24	50	49

DME: dimethyl ether.

Table 6. Liquid length (L_{liq}) [z/D] as a function of mesh density.

Mesh/smallest cell size	31 μm	62 μm	125 μm
Diesel	153.3	143.3	153.3
Methanol	122.2	127.8	140
n-dodecane	127.8	125.6	135.6
DME	54.4	75.6	65.5
Propane	34.4	64.4	44.4

DME: dimethyl ether.